Collapse of elongated voids in porous energetic materials: Effects of void orientation and aspect ratio on initiation

Nirmal Kumar Rai,[1] Martin J. Schmidt,[2] and H. S. Udaykumar[1]
[1]*Department of Mechanical and Industrial Engineering, University of Iowa, Iowa City, Iowa 52242, USA*
[2]*AFRL-RW, Eglin Air Force Base, Florida 32542, USA*
(Received 2 December 2016; published 28 April 2017)

The sensitivity of porous energetic materials depends on mesostructural heterogeneities such as voids, defects, cracks, and grain boundaries. The mesostructure of pressed explosives contains voids of arbitrary shapes including elongated voids of various orientations and aspect ratios. Mesoscale simulations to date have analyzed the effect of void morphology on the sensitivity of energetic materials for idealized shapes such as cylindrical, conical, and elliptical. This work analyzes the sensitivity behavior of elongated voids in an HMX matrix subject to shock loading. Simulations show that sensitivity of elongated voids depends strongly on orientation as well as aspect ratio. Ranges of orientations and aspects ratios are identified that enhance or inhibit initiation. Insights obtained from single elongated void analyses are used to identify sensitive locations in an imaged mesostructure of a pressed explosive sample.

DOI: 10.1103/PhysRevFluids.2.043201

I. INTRODUCTION

Heterogeneous energetic materials find applications in many engineering systems such as propulsive devices, munitions, and actuators. They are formulated by blending energetic crystals with plastic binders or physically pressing energetic crystals to form pressed pellets. Pressed energetic materials [1] are generally highly sensitive. However, their sensitivity can vary based on the mesostructural morphology in the formed pellet. The mesostructure of pressed explosives consists of energetic crystals and voids (in the form of crystal boundaries, defects, etc.). It is well established that the interaction of a shock wave with these mesostructural heterogeneities can lead to the formation of hot spots [2,3]. Chemical reactions and heat release are initiated at such hot spot locations and grow into the surrounding material. There are various mechanisms [3] through which hot spots can originate, such as void collapse, frictional heating between the energetic crystals, adiabatic shear banding, etc. Among these mechanisms, void collapse is considered to be predominant in the shock initiation regime [4–8].

Mesoscale simulations have been used in the past [4–12] to understand the effect of mesostructural heterogeneities on the sensitivity behavior of energetic materials. Several groups have performed simulations of void collapse; voids have often been assumed to assume an idealized shape such as cylindrical, spherical, and conical. The effects of void shape have been examined to a limited extent in previous work, suggesting that some void morphologies can lead to stronger hot spots than others [5,8,11,12]. Most of the previously studied shapes were modest deviations from spherical or cylindrical void shapes. However, as seen in a real (imaged) mesostructure of a pressed explosive (Fig. 1), voids are arbitrarily shaped and a large number of them can be elongated in shape. This work is an attempt to understand the sensitivity behavior of such elongated voids under shock loading. A further objective is to connect the collapse behavior and hot spot intensities of elongated voids with the initiation sensitivity of a real (i.e., imaged) porous explosive.

The phenomenon of void collapse has been extensively studied in the past via experimental studies [13–15] and numerical simulations [4–12], but the focus has been limited to the study of idealized shape voids such as cylindrical, elliptical, conical, or spherical voids. There are no experimental works that consider the study of noncylindrical voids such as those shown in the real mesostructure of the pressed explosives (Fig. 1). Also, there have been sparse attempts made to

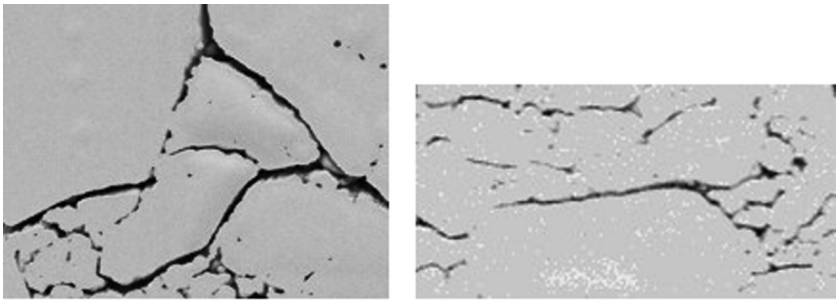

(a) (b)

FIG. 1. SEM image of the mesostructure of the pressed explosives samples. Two different types of pressed explosives are shown: (a) class III and (b) class V pressed energetic material explosive samples. Class III is a coarse-grained explosive and class V is a fine-grained explosive.

analyze the behavior of noncircular voids using mesoscale simulations [5,8,10–12]. In these works, limited attempts were made to study the effect of void morphology on the sensitivity of energetic materials using both inert and reactive mesoscale simulations. Notable early work includes Ref. [5], where inert calculations were performed on spherical and triangular or conical voids in HMX. It was observed that the spherical void produced a low-strength hot spot as compared to the triangular void. Also, the triangular void with its apex pointed towards the shock wave generated a low-strength hot spot as compared to a triangle with its base pointing towards the incident shock. Levesque and Vitello [8] also analyzed the effect of void morphology on the hot spot temperature for TATB using inert mesoscale simulations. Spherical, cylindrical, elliptical, and conical or triangular voids were considered in their study. Size effects of each of these void geometries were also studied. It was shown that elliptical and cylindrical voids, when arranged in line with their longest dimension (i.e., along the major axis for the elliptical void and along the length for the cylindrical void), produced much stronger hot spots than the spherical void for the same shock strength and volume fraction. Also, in agreement with Tran and and Udaykumar's [5] work, conical voids facing their apex towards the incident shock were found to be less sensitive when compared to the case where the base of the cone faced the incident shock. Levesque and Vitello [8] pointed out that void morphology has a significant effect on the hot spot temperature and that spherical voids must be recognized as idealized shapes when discussing the sensitivity of porous energetic materials. Although the inert mesoscale simulations have been able to illustrate the effect of various void morphologies on the hot spot temperature, they cannot yield insight into whether sustained reactions can originate from a given hot spot. This requires reactive mesoscale calculations.

Reactive mesoscale simulations have recently been employed to study the effect of void morphology on the sensitivity of energetic materials. Kapila *et al.* [11] performed reactive simulations on three different void shapes, spherical, prolate spheroid (long void), and oblate spheroid (tall void), in HMX. The effect of size of the three above-mentioned void shapes was also studied. It was observed that small-size voids are not sufficient for initiating reactions. Among the three void shapes, the oblate spheroid (tall void) was found to be most efficient in the generation of high strength that can lead to detonation. The recent work by Springer *et al.* [12] analyzed the effect of void morphology on the shock initiation and reaction rate in HMX. Spherical, elliptical, and conical voids were considered in the analysis. It was shown that elliptical and conical voids of high aspect ratio lead to increased sensitivity. Also, the effect of void morphology is shown to be dominant in the low-shock-pressure loading situations. It is clear from these mesoscale studies that void shape plays a crucial role in the sensitivity of porous energetic materials.

In past mesoscale efforts, although different shapes and size effects were analyzed, few studies directly correlated these effects to the behavior of a real mesostructure of an explosive. One such attempt is a recent work [10] that analyzed the response to shock loading of imaged mesostructures

and correlated the orientation of the elongated voids to initiation sensitivity. However, that study did not comprehensively cover the effect of various aspects of void morphology on sensitivity. Also, the grid resolution used in the study [10] was perhaps inadequate to accurately capture all aspects of the dynamics of slender voids. In the real mesostructures, voids of arbitrary shape and sizes are present. Figure 1 shows the scanning electron microscopy (SEM) image of two pressed explosive mesostructures classified as coarse-grained class III explosives and fine-grained class V explosives. It can be seen that the majority of the voids present in the mesostructure are of elongated shapes with various aspect ratios and orientations. In this work, using high-resolution numerical simulations, the effect of void morphology of elongated voids is investigated in detail; insights are obtained into the key geometrical features that influence sensitivity, i.e., void orientation and aspect ratio.

The work presented in this paper is arranged as follows. Section II presents a brief description of the governing equations, HMX material models, HMX reactive kinetics model, and the numerical framework of a massively parallel Eulerian code SCIMITAR3D [16,17]. Section III describes the computational setup used in the mesoscale analysis of the elongated voids. Section IV presents the key results of the mesoscale analysis by examining the effect of orientation and aspect ratio of elongated voids. The understanding obtained from the numerical experiments of elongated voids is then used to explain the initiation behavior of an imaged class III pressed energetic sample.

II. FORMULATION

In the current Eulerian framework, the governing equations are comprised of a set of hyperbolic conservation laws [18] corresponding to the conservation of mass, momentum, and energy:

$$\frac{\partial \rho}{\partial t} + \operatorname{div}(\rho \vec{V}) = 0, \tag{1}$$

$$\frac{\partial \rho \vec{V}}{\partial t} + \operatorname{div}(\rho \vec{V} \otimes \vec{V} - \sigma) = 0, \tag{2}$$

$$\frac{\partial \rho E}{\partial t} + \operatorname{div}(\rho E \vec{V} - \sigma \vec{V}) = 0, \tag{3}$$

where $\vec{V}$ is the velocity, ρ is the density, E is the specific internal energy, and σ is the Cauchy stress tensor. The stress state of material σ can be decomposed into a deviatoric part S and dilatational part P,

$$\sigma = S - PI. \tag{4}$$

The deviatoric stress S is obtained from the evolution equation in the rate form, by first updating the elastic response

$$\frac{\partial \rho S}{\partial t} + \operatorname{div}(\rho \vec{V} S) + \frac{2}{3}\rho G \operatorname{tr}(D) I - 2\rho G D = 0, \tag{5}$$

where D is the strain rate tensor and G is the shear modulus of the material. This step is followed by a radial return to the yield surface to account for plasticity. Further details on the elastoplastic treatment can be found in previous papers [16,17].

In the current work the energetic material considered is HMX. The constitutive and reactive models of HMX used in the current framework are discussed in the following paper [19]. The governing equations of mass [Eq. (1)], momentum [Eq. (2)], and energy [Eq. (3)], along with the evolution of deviatoric stresses, are spatially discretized using a third-order essentially nonoscillatory scheme [20] and numerically integrated using third-order Runge-Kutta time stepping. The interfaces in the current framework are handled using the narrow-band level set approach [21]. The level set approach allows for tracking of the interfaces in a sharp manner and can handle a large deformation

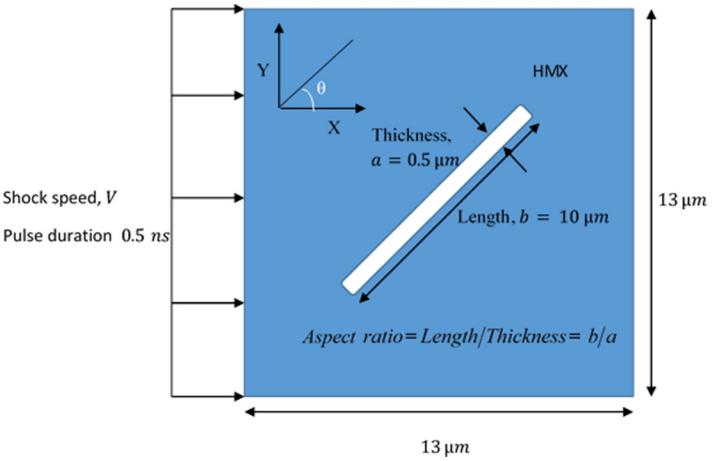

FIG. 2. Computational setup for the mesoscale simulations of the elongated void. An elongated void with thickness $a = 0.5\,\mu$m and length $b = 10\,\mu$m is oriented at an angle θ with respect to the incident shock wave. A shock load of the prescribed particle speed and pulse duration of 0.5 ns is applied from the west face of the domain boundary. East, south, and north faces are modeled as outlet conditions.

of the materials as in the formation of material jets and collapse. Interfacial conditions are applied at the sharp interface locations using a modified ghost fluid method [22]. The complete description of the numerical framework can be found in previous work [16,17].

III. COMPUTATIONAL SETUP

The sensitivity behavior of elongated voids is studied using reactive mesoscale simulations. In the current work sensitivity is characterized as a function of the strength of the imposed shock. A single elongated void in an otherwise homogeneous HMX material is considered. Figure 2 shows an elongated void of thickness $a = 0.5\,\mu$m and length $b = 10\,\mu$m oriented at an angle θ with respect to the incident shock embedded in a uniform HMX matrix of size of $13 \times 10\,\mu\text{m}^2$. A shock load of prescribed strength and 0.5-ns pulse duration is applied at the west face of the domain boundary. The other domain boundaries including the east, north, and south faces are modeled with outlet conditions.

The geometrical aspects of elongated voids such as orientation with respect to the incident shock and aspect ratio are varied to understand how these features can affect sensitivity. The numerical setup shown in Fig. 2 remains the same for all the studies herein.

IV. RESULTS

Extensive verification and validation of the current numerical framework for voids of circular cross section are presented in the following paper [19]. In that paper the material models for HMX, the reactive kinetics models, and the temperatures reached after void collapse are carefully benchmarked against available numerical and experimental results. In this work the effect of orientation and aspect ratio on sensitivity of elongated voids is analyzed.

A. Grid convergence study for the elongated voids

Grid resolution plays a crucial role in the mesoscale simulations of porous energetic materials. In the following paper [19] the effect of grid resolution on reaction initiation is studied for the situation involving cylindrical voids. It is shown that the use of coarse grids underpredicts the hot spot temperature and leads to incorrect prediction of sensitivity. It is also shown that the grid

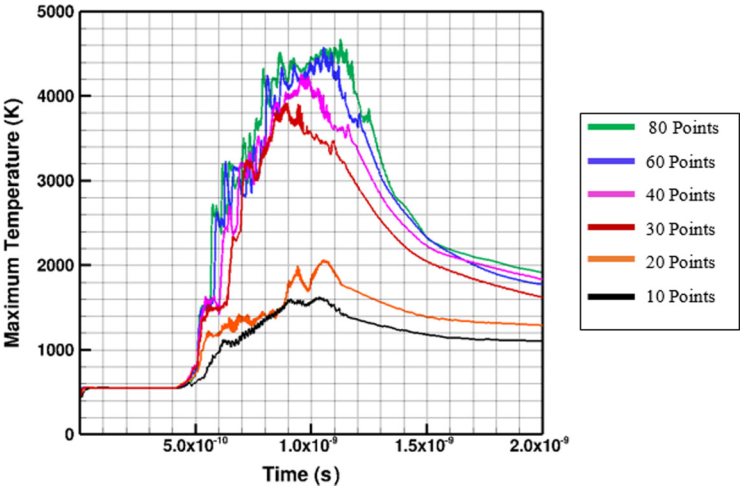

FIG. 3. Grid convergence study for the inert void collapse simulation. The study is performed for a single elongated void with a thickness of 0.5 μm and length of 20 μm in HMX material under a shock loading of 1000 m/s. Six different grid sizes corresponding to 10, 20, 30, 40, 60, and 80 grid points across the void thickness are considered.

resolution requirement for a cylindrical void depends on the shock strength. The grid resolution requirement becomes more stringent with increasing shock strength. For a cylindrical void, 700 grid points across the void diameter was found to be the required resolution; at that level of refinement, the uncertainty associated with the grid resolution on ignition prediction is sufficiently small. Apart from the shock strength, the grid resolution requirement can also be affected by the void morphology. The dependence of grid resolution on void morphology has not been studied in previous mesoscale work [4–8,10]. Without such a study it is not possible to assess whether a mesoscale simulation produces accurate predictions of sensitivity of a porous energetic material sample. In particular, as shown in Fig. 1, pressed explosives contain a distribution of elongated voids of various orientations and aspect ratios. Therefore, this section focuses on establishing the grid resolution required to obtain a converged solution for the void collapse of an elongated void.

The computational setup for the grid refinement study is shown in Fig. 2, with an elongated void oriented at an angle of $\theta = 45^\circ$ with respect to the incident shock. This first analysis is performed assuming HMX as an inert material, i.e., switching off the reaction calculation. In the following paper [19] involving cylindrical voids, it is observed that the grid resolution requirement becomes increasingly stringent with the increase in the shock strength. Therefore, for the elongated void the grid refinement study is performed for a high shock strength (1000-m/s particle velocity); lower-shock-strength cases will then demand a smaller number of grid points. An imposed shock corresponding to a particle velocity of 1000 m/s and pulse duration of 0.5 ns is applied at the west face of the domain boundary (Fig. 2). Six different grid sizes corresponding to 10, 20, 30, 40, 60, and 80 grid points across the thickness ($a = 0.5$ μm) of the elongated void are tested. The time variation of the maximum temperature in the domain is used as a measure through which grid convergence is established. Figure 3 shows the time variation of the maximum temperature for all six mentioned grid sizes. It can be seen that with the use of finer grids, the collapse temperature increases. The use of coarse grids, i.e., 10–20 grid points across the void thickness, significantly underpredicts the collapse temperature. With sufficiently fine grid sizes, i.e., 30–40 grid points across the void thickness, the collapse temperature starts to converge and eventually saturates for grid corresponding to 60 points across the void thickness. Therefore, in the rest of this paper, 40 points across the void thickness are used to resolve the elongated voids.

B. Effect of void morphology on the sensitivity behavior of energetic materials

Voids of circular and triangular cross sections have been used in the past to understand the behavior of porous energetic materials [4,6,7]. However, real mesostructure of explosives contain elongated or other irregularly shaped voids that may impact on the sensitivity of the porous material. The effect of elongated void shapes is studied by comparing the ignition threshold of a cylindrical void and an elongated void of the same effective void area using reactive mesoscale simulations.

There are multiple ways through which reaction initiation can be identified in a reactive mesoscale simulation. For example, the initiation of chemical reaction and ignition in HMX can be indicated by the rise in temperature due to the initiation of exothermic reactions. Ignition can also be tracked via the rise in the total specific internal energy of the mesoscale sample. The total specific internal energy is calculated as

$$e_T = \frac{\int_V \rho e \, dV}{\int_V \rho \, dV}, \tag{6}$$

where e_T is the total specific internal energy in the sample and e is the computed specific internal energy field. The total internal energy is a scalar quantity that tracks the conversion of mechanical energy to heat through plastic dissipation, material jetting, impact, and void collapse.

The reaction initiation and ignition in the material can also be indicated by the mass fraction of the final gaseous species. The volume average of the final gaseous species can be expressed as

$$F = \frac{\int_V \rho Y_4 dV}{\int_V \rho \, dV}, \tag{7}$$

where F is the volume average of the final gaseous species, Y_4 is the mass fraction of the gaseous species, and V is the volume.

The volume average of the final gaseous species over the domain indicates whether the reaction has been initiated, is partially completed, or is fully completed. Therefore, the volume average of the final gaseous species and total specific internal energy are used in this work to track reaction initiation and ignition.

1. Ignition threshold for an elongated void

The computational setup shown in Fig. 2 is used to obtain the ignition threshold of elongated voids. The void is oriented at an angle of $\theta = 45^\circ$ with respect to the incident shock. The shock pulse duration is kept constant at 0.5 ns for the study. Four different shock strengths, corresponding to particle velocities of 350, 500, 650, and 850 m/s, are considered.

The time variation of the total specific internal energy is analyzed. Figure 4(a) shows the rise in the specific internal energy as the collapse of the void leads to the formation of a hot spot for all of the shock speeds. However, two distinct situations can arise *after* hot spot formation. Depending on the temperature and the size of the hot spot formed after the collapse, the reaction can be initiated or the hot spot can be extinguished. For shock strengths of 350 and 500 m/s, the hot spot formed is not intense enough and diffusion redistributes the hot spot energy to the surroundings, leading to quenching of the hot spot. This is evident from Fig. 4(a), which shows that after the formation of the hot spot the total specific internal remains a constant. For shock strengths of 650 and 850 m/s, the hot spot formation is followed by reaction initiation and ignition in the material, which is indicated by the sharp rise of the total specific internal energy in Fig. 4(a).

As the shock strength increases, the strength of the hot spot formed also increases and it takes less time to initiate a reaction for a high-strength hot spot. This can be observed in Fig. 4(a), where the sharp rise in the total specific internal energy starts later for the 650-m/s shock and earlier for the 850-m/s shock. The threshold for the elongated void (Fig. 2) with thickness $a = 0.5\,\mu$m and length $b = 10\,\mu$m oriented at an angle of $\theta = 45^\circ$ with respect to the incident shock wave is observed to lie between 500 and 650 m/s.

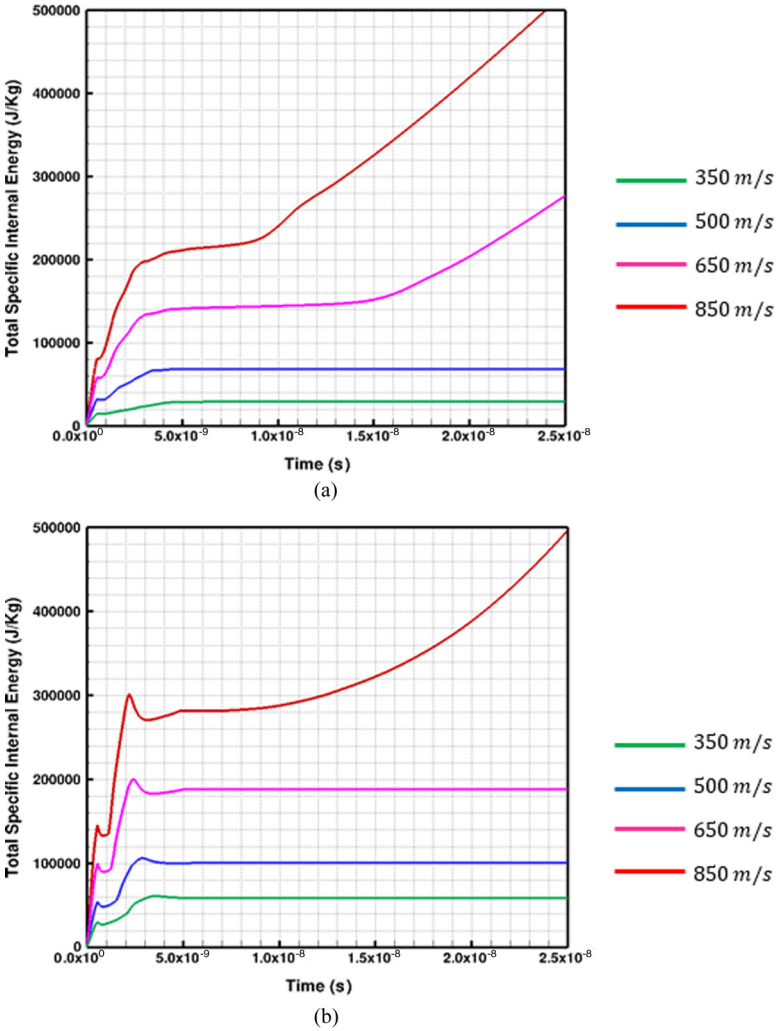

FIG. 4. Time variation of the total specific internal energy for different shock strengths of imposed particle speeds of 350, 500, 650, and 850 m/s. The results are obtained from the reactive mesoscale simulation of (a) an elongated void (Fig. 2) oriented at angle of 45° with respect to the incident shock wave and (b) a circular void of the same area as the elongated void. The diameter of the circular void is 2.52 μm. The loading pulse is kept constant at 0.5 ns for all the simulations.

2. Ignition threshold for a cylindrical void

The effect of the void shape can be examined by comparing the threshold of a cylindrical void of the same effective void area as the elongated void used in the previous case (Fig. 2). The void area of the elongated void used in the previous analysis was 5 μm^2, which corresponds to a diameter of 2.52 μm for the cylindrical void. Four different shock strengths with imposed particle speeds of 500, 650, 850, and 1000 m/s are used to identify the ignition threshold for the cylindrical void.

Figure 4(b) shows the time variation of the total specific internal energy. The 500-, 650-, and 850-m/s cases do not lead to initiation. This can be seen in Fig. 4(b), where the total specific internal energy settles to a constant value after the hot spot formation. For a 1000-m/s shock strength, the hot spot strength is sufficient to initiate a chemical reaction and the reaction initiation can be seen

in Fig. 4(b) through a sharp rise in the total specific internal energy. The ignition threshold of a cylindrical void of 2.52 μm is observed to lie between 850- and 1000-m/s shock speed.

3. Comparison of the sensitivity behavior of an elongated and cylindrical void

For the same void volume fraction of an elongated void oriented at an angle of $\theta = 45^\circ$ and a cylindrical void, the ignition threshold for the elongated void lies between 500 and 650 m/s and for cylindrical void it lies between 850 and 1000 m/s. This indicates that elongated voids at certain orientations are more sensitive than cylindrical voids. It is useful to understand the cause of the heightened sensitivity of the elongated void relative to the cylindrical void. Figure 5 compares the collapse behavior of the two voids under a shock load of 650 m/s and a pulse duration of 0.5 ns. The collapse of the cylindrical void starts with the formation of a strong material jet at the upstream surface of the void [Fig. 5(c)]. The material jet impacts the downstream surface of the void, leading to the formation of a primary blast wave and a local high-temperature zone at the point of jet impact [Fig. 5(c)]. The initial jet impact also causes the formation of two symmetrical lobes, i.e., secondary voids, which are formed from the initial cylindrical void [Fig. 5(c)]. These symmetrical lobes collapse under the combined influence of the initial shock load and the primary blast wave. The collapse of the symmetrical lobes causes a further rise in the hot spot temperature [Fig. 5(e)]. In fact, this secondary collapse temperature can be significantly higher than the initial temperature rise caused by the jet impact [Fig. 5(e)]. The reaction may be initiated either near the initial jet impact site or near the secondary collapse temperature, depending on the strength of the shock. For a shock speed of 650 m/s, the hot spot formed after both the primary and secondary collapses of the voids is unable to initiate a reaction and the hot spot diffuses [Fig. 5(g)]. The collapse of an elongated void oriented at $\theta = 45^\circ$ is different from the cylindrical void case, as shown in Fig. 5. The collapse of the elongated void involves successive pinching of the upstream surface of the void against the downstream surface [Figs. 5(b) and 5(d)], i.e., the jetting and impact mechanism does not operate in this case. Each pinching event causes the formation of a blast wave that strengthens with the continuing collapse along the length of the void [Fig. 5(d)]. With each pinching instance the strength of the resulting blast increases. This intensification subsequently pinches the void under increased shock loads and causes the formation of successively-higher-strength hot spots [Fig. 5(f)]. The hot spot formed after the collapse of the elongated void is thereby able to initiate a chemical reaction [Fig. 5(h)]. This self-strengthening mechanism of the shock is present only in the elongated void situation and not present in the collapse of cylindrical voids. Therefore, for a given void area the elongated void is more sensitive than the corresponding cylindrical void.

C. Effect of orientation of elongated voids on sensitivity of pressed energetic materials

The real mesostructure of pressed energetic materials (Fig. 1) contains elongated voids of various orientations and aspect ratios. The orientation of elongated voids can significantly affect the sensitivity behavior of energetic materials, as indicated in the work of Levesque and Vitello [8]. Therefore, the next part of this study seeks to quantify the effect of orientation of elongated voids on the ignition threshold of energetic materials and to obtain physical insights into the effect of orientation. The computational setup shown in Fig. 2 is used to study the effect of orientation. The orientation is prescribed with respect to the incident shock wave. Five different orientations are considered, i.e., $\theta = 0^\circ$, 30°, 45°, 60°, and 90°. The void thickness and length are maintained constant for all the orientations (Fig. 2). The shock pulse duration is maintained at 0.5 ns. As shown in Sec. IV B 1, the threshold for the elongated void oriented at an angle of $\theta = 45^\circ$ lies between 500 and 650 m/s. Based on this observation, a shock strength of 650 m/s is used in the current analysis to examine the relative sensitivity of other orientations. Figure 6 shows the time variation of the total specific internal energy and the volume averaged mass fraction of the final gaseous species for the five orientations. It can be seen that for the elongated voids oriented at angles of $\theta = 0^\circ$, 30°, and 45°, there is sharp rise in the total specific internal energy (due to sustained chemical reactions) after the initial peak generated by the collapse of the elongated voids [Fig. 6(a)]. Also, the volume mass

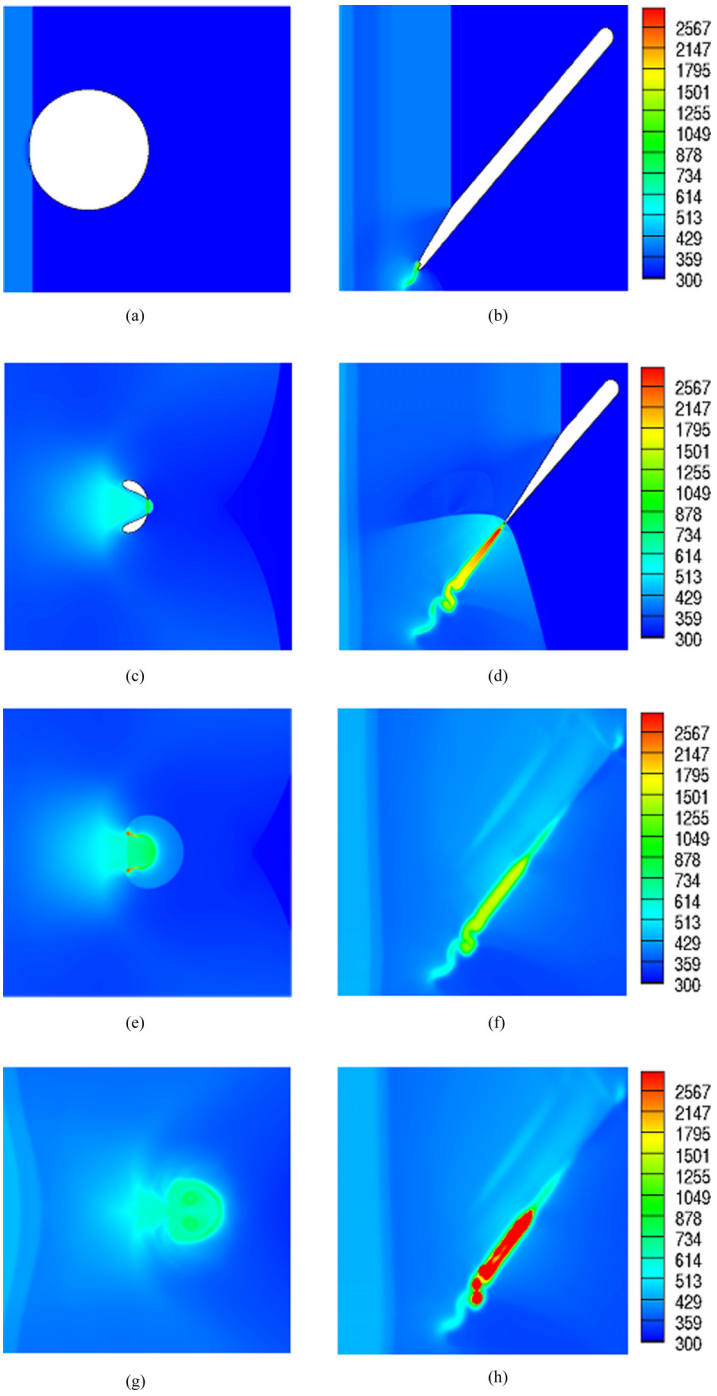

FIG. 5. Contour plots of temperature (K) at different instants of time for the reactive mesoscale simulations of a cylindrical void and an elongated void oriented at an angle of 45° with respect to the incident shock load: (a) $t = 0.37$ ns, (b) $t = 0.83$ ns, (c) $t = 1.56$ ns, (d) $t = 1.62$ ns, (e) $t = 1.7$ ns, (f) $t = 3.71$ ns, (g) $t = 4.85$ ns, and (h) $t = 19.07$ ns. The elongated void is 0.5 μm thick and 10 μm long. The diameter of the cylindrical void is 2.52 μm. The void area of the elongated void and the cylindrical void is same. The shock load with a particle speed of 650 m/s and pulse duration of 0.5 ns is applied from the west face of the domain.

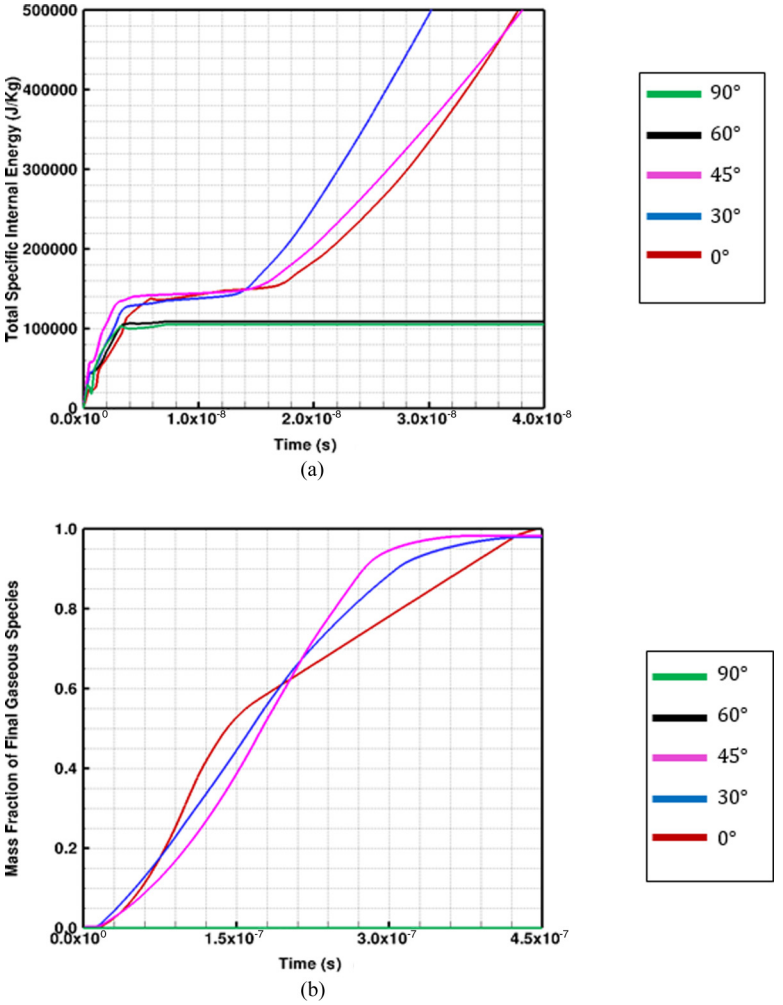

FIG. 6. Time variation of (a) the total specific internal energy and (b) the volume-averaged mass fraction of the gaseous species for different shock strengths of 650 m/s and pulse duration of 0.5 ns. The results are obtained from the reactive mesoscale simulation of an elongated void (Fig. 2). The effect of orientation of the elongated void is studied by studying five different orientations: 0°, 30°, 45°, 60°, and 90°. The orientation is prescribe with respect to the incident shock wave.

fraction of the final gaseous species increases and reaches a value of 1, indicating complete burning in the material [Fig. 6(b)]. For elongated voids oriented at angles of $\theta = 60^\circ$ and 90° the strength of the hot spot formed after the collapse of the elongated void is not sufficient to initiate a reaction and the hot spot is quenched. This is indicated in the total specific internal energy plot [Fig. 6(a)]. Therefore, the critical orientations for which an elongated void is sensitive lie between 0° and 45° for the given loading conditions.

Next we seek to understand why the elongated voids oriented at angle that lies between 0° and 45° are more sensitive than other orientations. Figure 7 shows the comparison between the temperature fields generated during the collapse of voids oriented at angles of 0° and 90°. The major axis of the 0° void aligns with the direction of the shock travel [Fig. 7(a)] as compared to the 90° void, where it is perpendicular to the direction of shock travel [Fig. 7(b)]. For the 0° void, the incident shock causes a pinching action and generates high-temperature hot spots [Fig. 7(c)]. For the 90° void, the

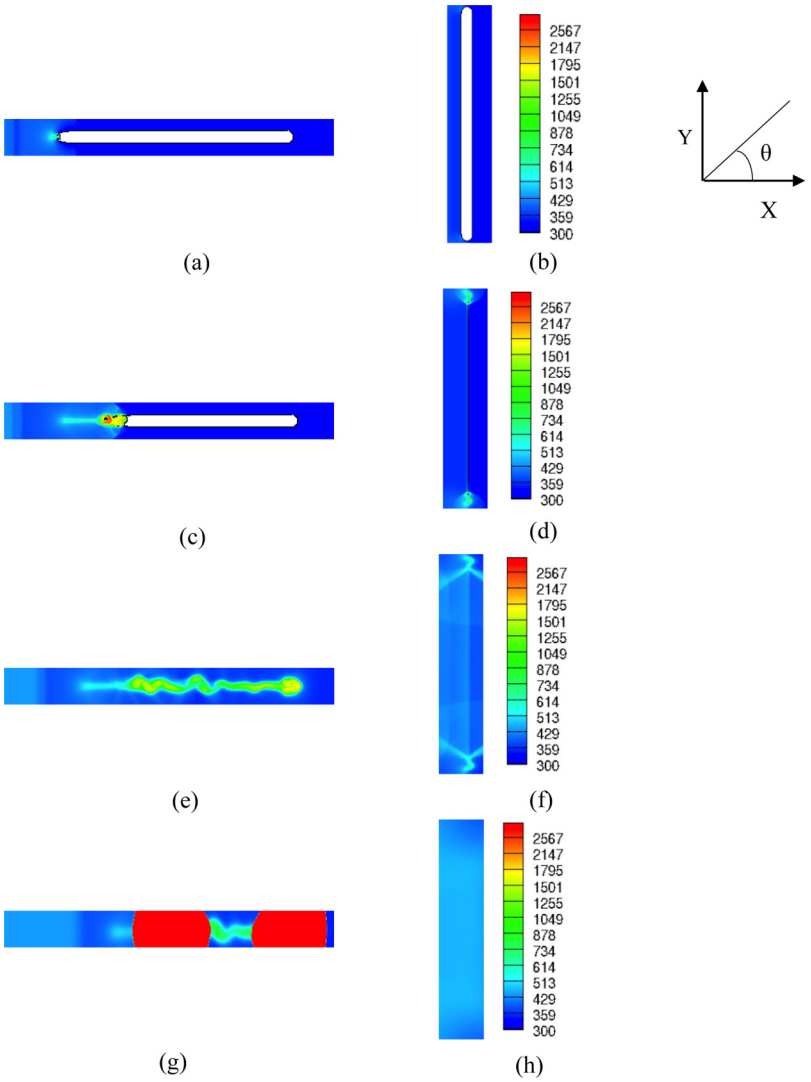

FIG. 7. Temperature (K) contour plots at different instants of time showing the difference in the reaction initiation behavior of two elongated voids with a thickness of 0.5 μm and length of 10 μm oriented at angles of 0° and 90° with respect to the shock load: (a) $\theta = 0°$ void at $t = 0.68$ ns, (b) $\theta = 90°$ void at $t = 0.45$ ns, (c) $t = 1.37$ ns, (d) $t = 0.73$ ns, (e) $t = 11.58$ ns, (f) $t = 1.2$ ns, (g) $t = 86.3$ ns, and (h) $t = 2.32$ μs. The shock speed for the analysis is maintained at 650 m/s and the pulse duration is 0.5 ns.

shock impacts the upstream surface of the void and reflects as a rarefaction wave [Fig. 7(d)]. The rarefaction wave cools down the hot spot formed after the collapse and no reaction is observed for the 90° void. The rarefaction effect is not present for the 0° void as the shock wave propagation aligns with the length of the void [Fig. 7(g)]. This observation is in agreement with Ref. [8], where it is shown that elongated shapes aligned with the direction of shock propagation cause the formation of stronger hot spots.

As the orientation of the void is increased from 0° towards 90° the ability of the rarefaction wave to cool the hot spot also increases. Figure 8 shows this effect by comparing the temperature contour plots for three other orientations, viz., 30°, 45°, and 60°. The pinching mechanism of the void collapse to produce higher-strength hot spots dominates until the orientation reaches 45°. This

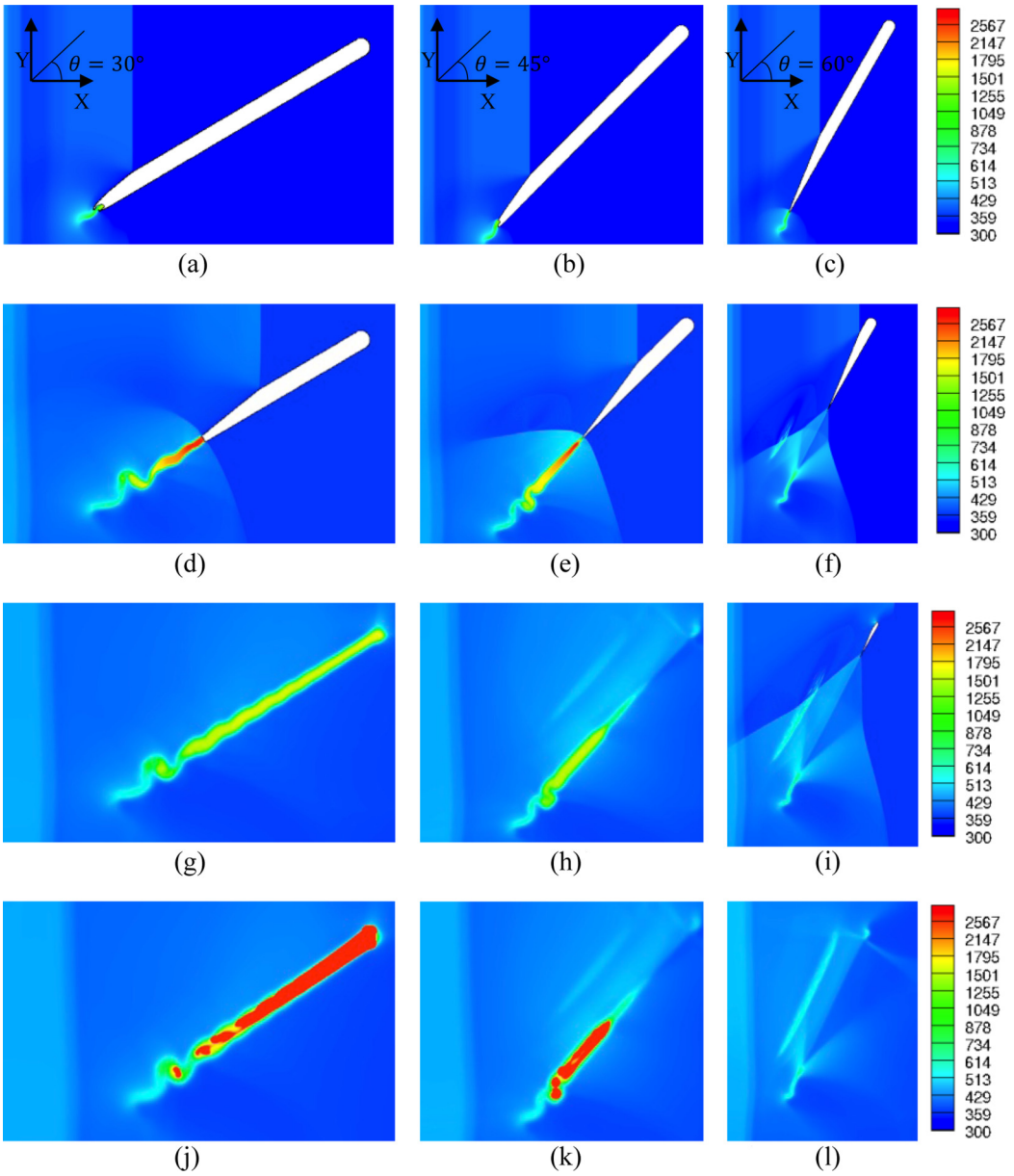

FIG. 8. Temperature (K) contour plots at different instants of time showing the difference in the reaction initiation behavior of three elongated voids with a thickness of 0.5 μm and length of 10 μm oriented at angles of 30°, 45°, and 60° with respect to the shock load: (a) $t = 0.83$ ns, (b) $t = 0.83$ ns, (c) $t = 0.87$ ns, (d) $t = 1.66$ ns, (e) $t = 1.61$ ns, (f) $t = 1.39$ ns, (g) $t = 3.9$ ns, (h) $t = 3.7$ ns, (i) $t = 1.74$ ns, (j) $t = 20.2$ ns, (k) $t = 19.1$ ns, and (l) $t = 3.81$ ns. The shock speed for the analysis is maintained at 650 m/s and the pulse duration is 0.5 ns.

causes reaction initiation for the 30° [Fig. 8(j)] and the 45° voids [Fig. 8(k)]. With a further increase in orientation to 60°, the rarefaction effect dominates and cools down the hot spot, thereby preventing reaction initiation [Fig. 8(l)]. There is therefore a competition between the pinching mechanism of the void and the rarefaction-induced cooling during the collapse of elongated voids; as the orientation

increases towards 90° the rarefaction effect tends to dominate. The pinching mechanism dominates for an orientation of less than 45°, causing the voids to be more sensitive in the range of 0°–45°.

D. Effect of aspect ratio of elongated voids on sensitivity

The previous cases analyzed the effect of the void orientation on the sensitivity of HMX. Along with the orientation, the aspect ratio of an elongated void can affect the sensitivity of the porous energetic materials. The aspect ratio in the context of the current analysis is defined as the ratio of the length of the void to its thickness, as illustrated in Fig. 2. The aspect ratio for the elongated void shown in Fig. 2 is 20. The orientation of the void with respect to the incident shock wave is kept constant at $\theta = 45^\circ$. The shock loading with an imposed particle speed of 650 m/s and pulse duration of 0.5 ns is applied from the west face of the boundary. A shock strength of 650 m/s is used in the current analysis because the ignition threshold for the elongated void with an aspect ratio of 20 and oriented at an angle of 45° was observed to lie between 500 and 650 m/s. The aspect ratio of the void is varied by keeping the void area constant at 5 μm^2. Six different aspect ratios are used, corresponding to 2, 3, 5, 10, 15, and 20.

Figure 9 shows the time variation of the total specific internal energy and the volume-averaged mass fraction of the final gaseous species for all six void geometries. For the same void volume fraction and shock loading, the voids with smaller aspect ratios, i.e., less than 5, do not produce sustained reactions and the hot spot formed from the collapse of the void is quenched. This can be seen in Fig. 9, where the total specific internal energy rises because of the formation of the hot spot and eventually settles down to a constant value. Also, the mass fraction of the gaseous species does not increase with time, indicating nonreactive cases. For the voids with aspect ratios greater than 5, the hot spot formed after the collapse leads to the initiation of chemical reactions, indicated by the sharp rise in the total specific internal energy [Fig. 9(a)]. Also, the mass fraction of the gaseous species increases and reaches a value of 1, showing ignition and complete burning of the HMX material [Fig. 9(b)]. Therefore, thicker voids (low aspect ratios) are less sensitive than thinner voids (large aspect ratio). The critical aspect ratio lies above the value of 5 for the given loading conditions and void orientation. Note that the critical aspect ratio will depend on shock loading as well as on orientation.

In the above simulations, thicker voids are found to be less sensitive than thinner voids. Figures 10 and 11 seek to understand the mechanisms underlying this observation by showing the deformation profile of voids of different aspect ratios. Figure 10 compares the time variation of the temperature contour plots of voids with aspect ratios of 2 and 10. The void with an aspect ratio of 2 undergoes collapse by the formation of an asymmetrical material jet [Figs. 10(c) and 10(e)]. The void with an aspect ratio of 10 undergoes collapse by the pinching mechanism leading to the successive collapse of the void. It was shown in Sec. IV B 3 that the pinching mechanism produces higher-temperature hot spots than the collapse under material jetting by comparing the behavior of a cylindrical and an elongated void. This difference in the mode of collapse, i.e., jetting versus pinching, causes the sensitivity of thicker voids to be low when compared to the thin voids.

The physical mechanism governing the collapse of elongated voids transitions from material jetting to a pinching mechanism as the aspect ratio of the void is increased. This transition is demonstrated in Fig. 11 by comparing the numerical schlieren plots for three aspect ratios, viz.,2, 5, and 10. The void with an aspect ratio of 2 deforms because of the formation of a material jet [Fig. 11(d)]. The shock focusing due to the jet increases as the deformation of the void progresses [Fig. 11(g)], leading to final collapse [Fig. 11(j)]. When the aspect ratio is increased to 5, initially the void starts to deform but there is no pinching action involved at the start of void collapse [Fig. 11(e)]. As the void starts to deform further the pinching action comes into play [Fig. 11(h)], leading to the complete collapse of the void. Further increasing the aspect ratio to 20 causes the void to collapse because of the pinching mechanism [Fig. 11(f)] and successive pinching events continue until the void collapses completely [Fig. 11(i)]. It can be seen that the transition of the physical mechanism from material jetting to pinching takes place as the aspect ratio is increased. Voids of aspect ratio 5 can be identified as the threshold where this transition is most evident. For thicker voids, the surface

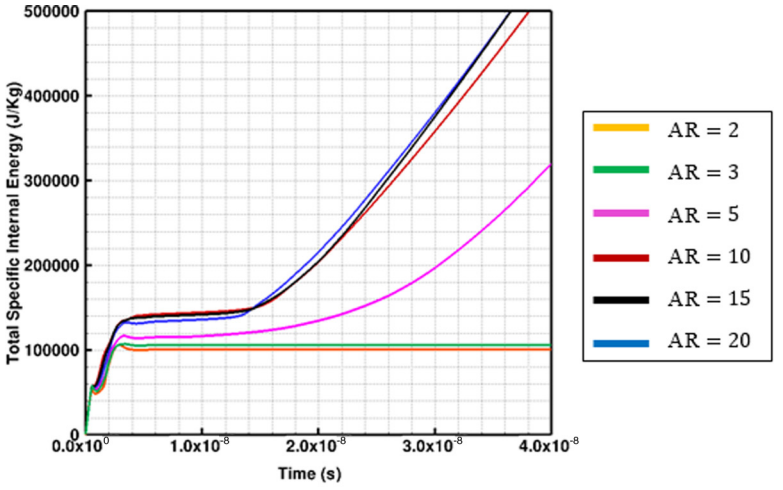

(a)

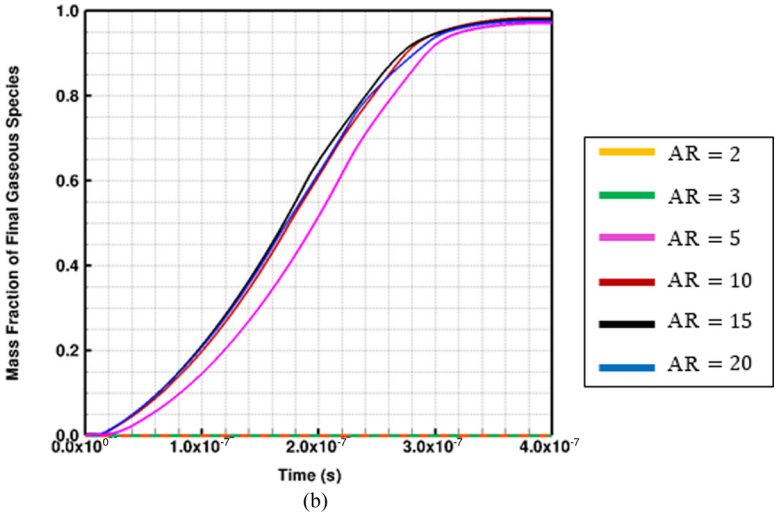

(b)

FIG. 9. Time variation of (a) the total specific internal energy and (b) the volume-averaged mass fraction of the gaseous species for different shock strengths of 650 m/s and pulse duration of 0.5 ns. The results are obtained from the reactive mesoscale simulation of an elongated void (Fig. 4) oriented at an angle of 45° with respect to the incident shock wave. The effect of orientation of the elongated void is studied by studying six different aspect ratios (AR) of value 2, 3, 5, 10, 15, and 20. The AR is defined as the ratio of length to thickness.

area of the void that interacts with the incident shock initially is high, which allows sufficient time for the formation of a material jet. For thinner voids, the surface area impacted by the incident shock wave is small, causing the immediate collapse by a pinching action. The series of pinching actions creates a high-strength hot spot and makes the thinner voids more sensitive.

E. Shock analysis of class III pressed explosive sample

The current study has identified the key morphological features of elongated voids that cause the voids to exhibit greater sensitivity. The insights obtained from the numerical experiments above, with regularly (analytically) shaped elongated voids, can help in the understanding of the initiation

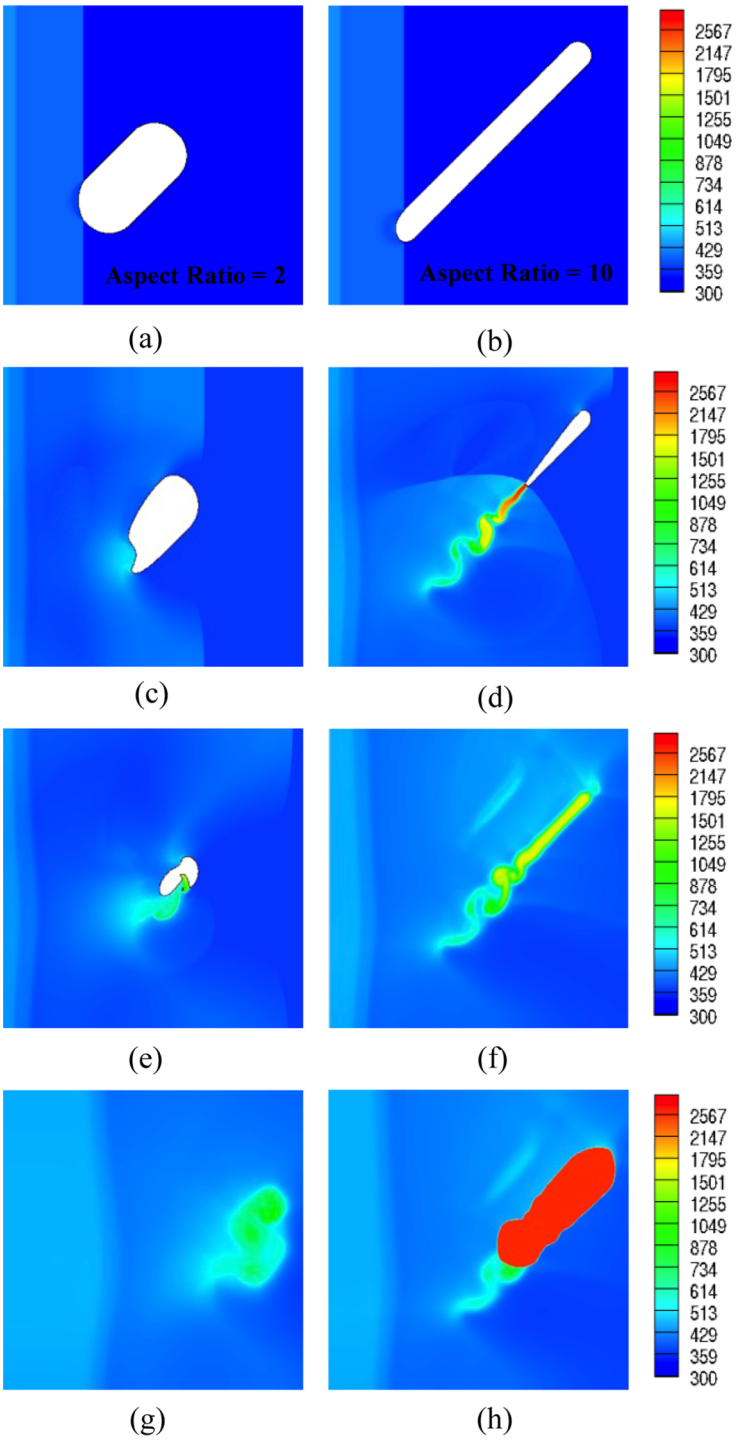

FIG. 10. Temperature contour plots for the two elongated void with aspect ratios 2 and 20: (a) $t = 0.46$ ns, (b) $t = 0.45$ ns, (c) $t = 1.07$ ns, (d) $t = 1.7$ ns, (e) $t = 1.5$ ns, (f) $t = 2.8$ ns, (g) $t = 11.02$ ns, and (h) $t = 37.8$ ns. The voids are oriented at an angle of 45° with respect to the shock wave. The computational setup is shown in Fig. 2. The shock strength is 650 m/s and the pulse duration is 0.5 ns.

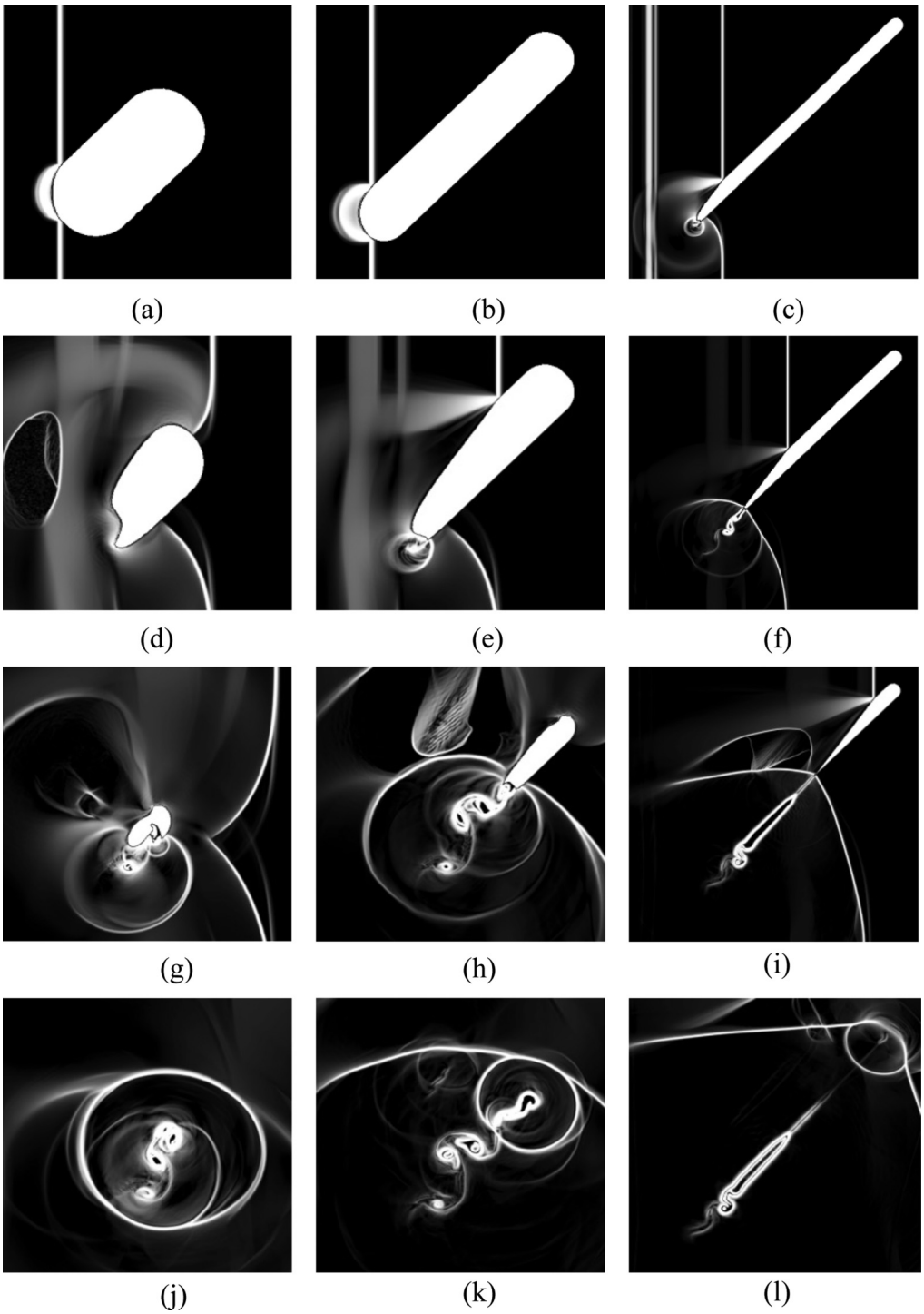

FIG. 11. Numerical schlieren plots for three elongated voids with aspect ratios 2, 5, and 20: (a) $t = 0.46$ ns, (b) $t = 0.46$ ns, (c) $t = 0.7$ ns, (d) $t = 1.07$ ns, (e) $t = 0.96$ ns, (f) $t = 1.17$ ns, (g) $t = 1.54$ ns, (h) $t = 1.6$ ns, (i) $t = 1.82$ ns, (j) $t = 2.05$ ns, (k) $t = 2.2$ ns, and (l) $t = 2.66$ ns. The voids are oriented at an angle of 45° with respect to the shock wave. The computational setup is shown in Fig. 2. The shock strength is 650 m/s.

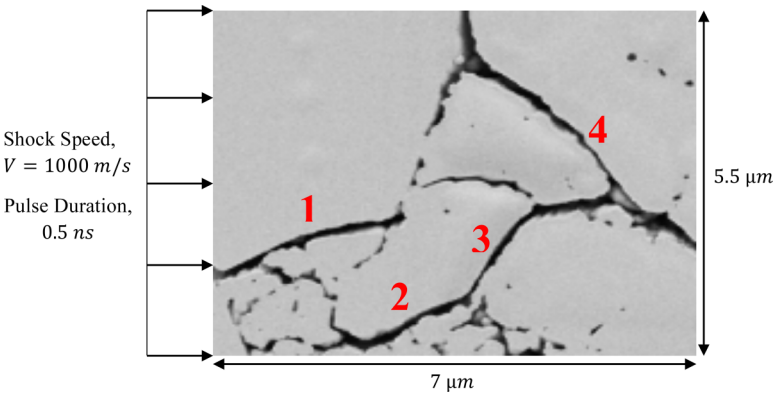

FIG. 12. Numerical setup for reactive mesoscale analysis of a class III pressed explosive sample. The sample size is $7 \times 5.5\,\mu\text{m}^2$. A shock load with a particle speed of 1000 m/s and pulse duration of 0.5 ns is applied from the west face of the domain boundary. There are four voids marked in the mesostructure of the sample numbered from 1 to 4 based on the orientations and aspect ratio.

behavior of real (imaged) pressed explosive samples (Fig. 1). This can also help in the development of the ability to predict the locations in the pressed samples where critical hot spots can occur. To demonstrate this, shock simulations of the class III pressed HMX sample [shown in Fig. 1(a)] are performed.

Figure 12 shows the computational setup for the analysis of the class III sample. Shock loading with a strength of 1000 m/s and pulse duration of 0.5 ns is applied from the west face of the domain. The other faces of the domain boundary are modeled as outlet boundaries. The SEM image of the class III sample is processed using the image processing algorithms implemented in SCIMITAR3D [10,23]. Speckle reducing anisotropic diffusion is used to denoise the image and an active contouring algorithm is used for image segmentation to obtain a level set representation of the voids present in the mesostructure. The image processing algorithms have been presented in detail and validated in previous work [10,23].

Based on the simulations above, the critical orientation lies between 0° and 45° and the critical aspect ratio is greater than 5. In Fig. 12 a small number of voids that lie outside these mentioned ranges of orientation and aspect ratio are tagged (numbered 1–4 in Fig. 12). The void at location 1 is oriented approximately at an angle of 30°–45°, at location 2 it is oriented at an angle of 20°–30°, at location 3 the void is oriented at an angle of 50°–70°, and the void at location 4 is oriented at angle of 135° (−45°) with respect to the shock wave. All the four voids have high aspect ratios (i.e., they are thin voids). It will be shown that in this particular mesostructure of class III, the voids that have high aspect ratio and orientation play a key role in affecting the sensitivity of the sample to shock loading.

The voids at locations 1, 2, and 4 lie in the critical parameter range of orientation and aspect ratio; it can be expected that these are some of the critical locations where the reaction will be initiated. Void 3 lies outside the critical parameter range of orientation and it may be less sensitive. Shock analysis on the class III sample is performed to understand how closely the predictions hold up for all four locations. The grid resolution is decided based on the elongated void grid resolution study in Sec. IV A, i.e., 40 grid points are used across the void thickness. The void at location 1 is selected as a standard to maintain the grid resolution requirement in the full domain. Note that the void at location 1 was resolved by roughly five pixels across its thickness in the original SEM image. Therefore, by refining the computational grid by a factor of 8 times the original image resolution, 40 grid points across the void thickness were employed to enable reliable computations of the collapse.

Figure 13 shows the numerical schlieren plots at different instances of shock propagation showing the local deformation of voids and the formation of blast waves from successive collapse of the voids. The void at location 1 starts to collapse and due to the pinching action high strength blast waves [Figs. 13(b) and 13(c)] emanate from the collapse locations. The same is observed for the voids at

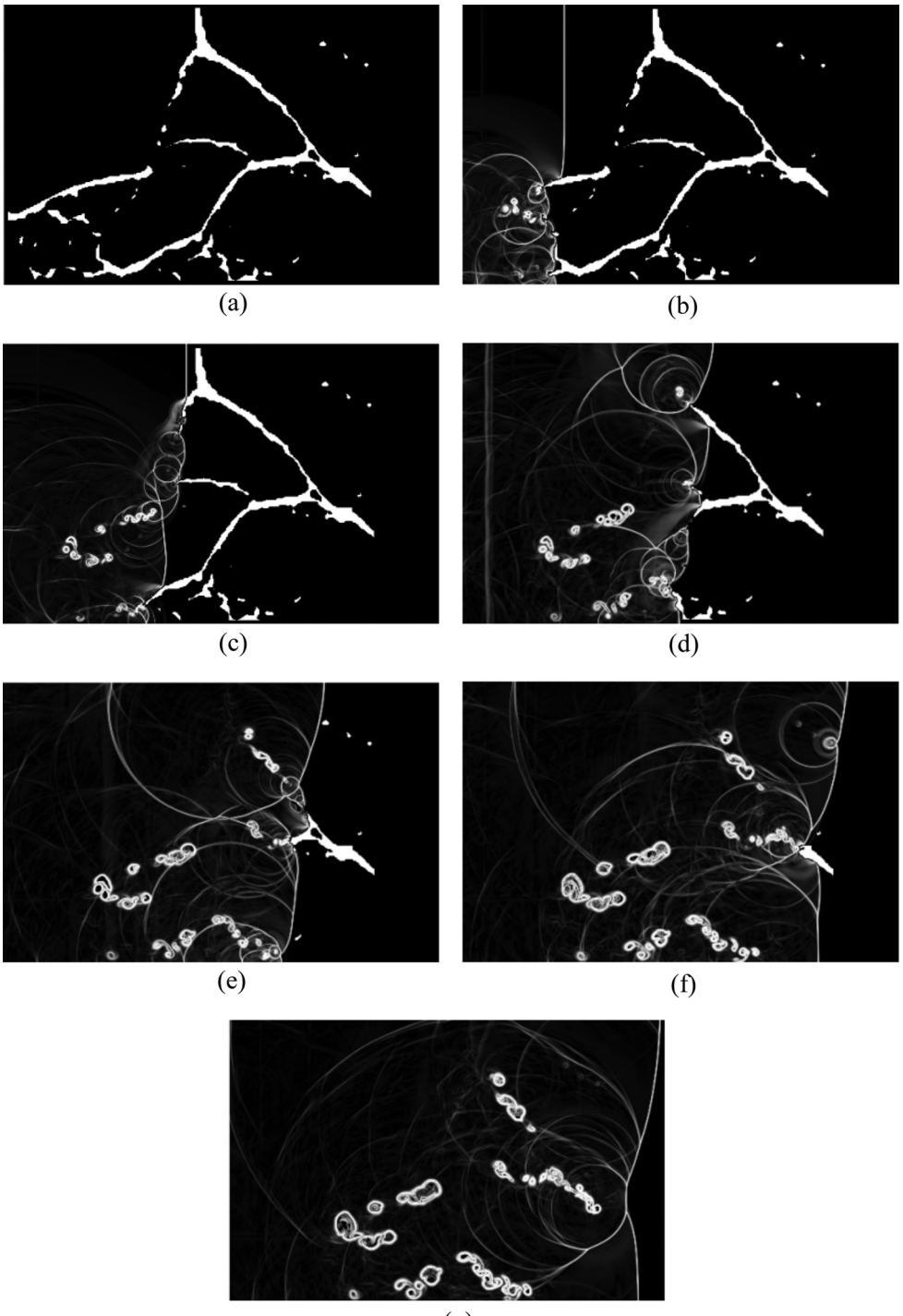

FIG. 13. Numerical schlieren plot for reactive mesoscale simulation of the class III pressed explosive sample under a shock loading of 1000 m/s and pulse duration of 0.5 ns: (a) $t = 0.0$ ns, (b) $t = 0.48$ ns, (c) $t = 0.86$ ns, (d) $t = 1.23$ ns, (e) $t = 1.55$ ns, (f) $t = 1.87$ ns, and (g) $t = 2.18$ ns. Schlieren indicate the formation of the blast waves and vortices because of the subsequent collapse of the elongated voids.

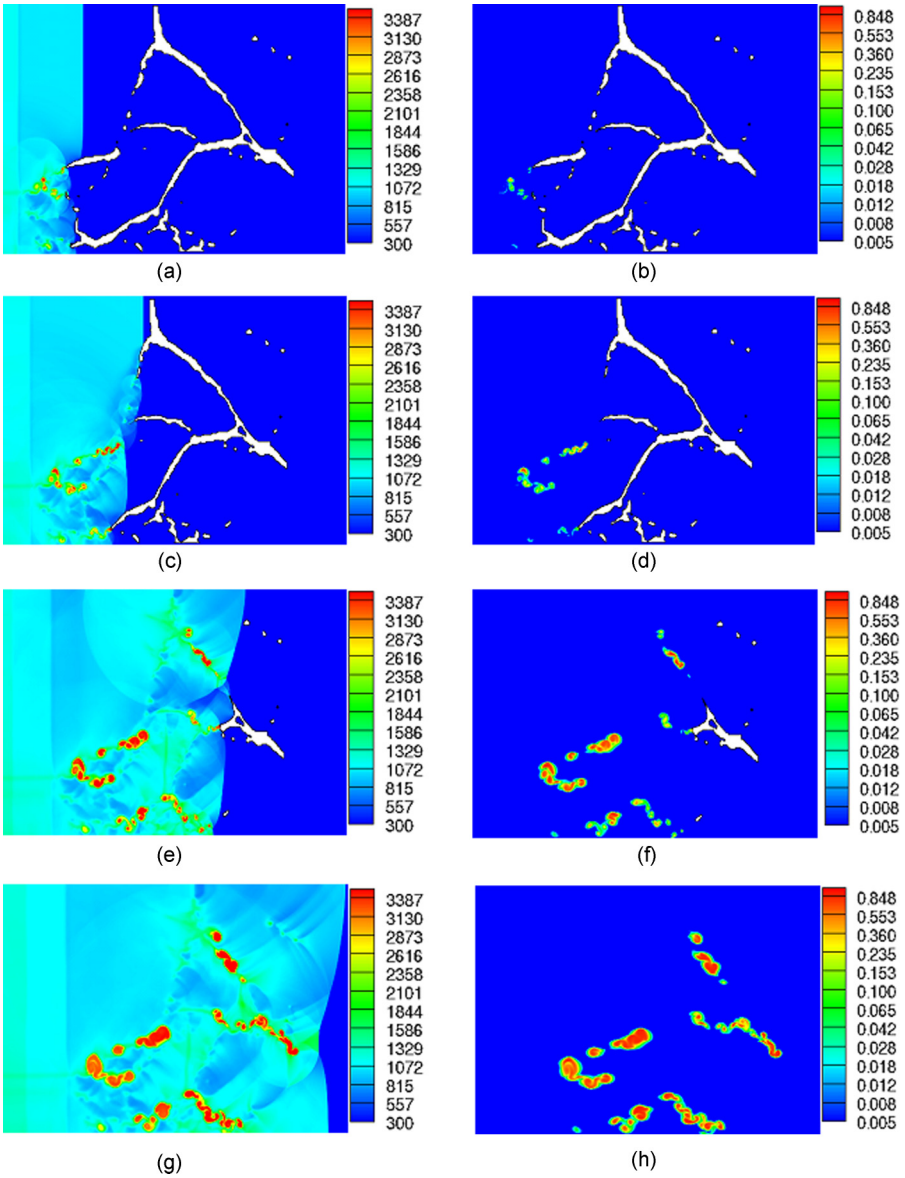

FIG. 14. Contour plot of temperature (K) at (a) $t = 0.48$ ns, (c) $t = 0.86$ ns, (e) $t = 1.5$ ns, and (g) $t = 2.18$ ns and the mass fraction of the final gaseous species at (b) $t = 0.48$ ns, (d) $t = 0.86$ ns, (f) $t = 1.5$ ns, and (h) $t = 2.18$ ns for the reactive mesoscale simulation of the class III pressed explosive sample under a shock loading of 1000 m/s and pulse duration of 0.5 ns. The reaction is initiated at the sensitive elongated void locations with critical values of orientations and aspect ratio.

locations 2 and 4 [Figs. 13(d) and 13(f)]. The collapse of the other voids surrounding void 2 causes the formation of a blast wave and there is a complex interaction of the blast waves formed from all the voids. This suggests strong void-void interactions between all the neighboring voids, as noted in the work of Kapahi and Udaykumar [7] in the context of cylindrical voids. The void at location 3 also collapses, but as can be seen in Fig. 13(f), the blast wave strength formed from its collapse is not sufficiently high and no reaction initiates at that location.

The reaction initiation and sensitivity of each of the four voids are elucidated using contour plots of the temperature and the mass fraction of final gaseous species (Fig. 14). Based on the predictions from the numerical experiments, the voids at locations 1, 2, and 4 are categorized as sensitive and the void at location 3 void is less sensitive. The void at location 1 creates a hot spot of sufficient strength and a reaction is initiated [Fig. 14(c)] locally at location 1. The reaction initiation can also be seen in the contour plot of the mass fraction of the gaseous species [Fig. 14(d)]. The same is observed for the voids at locations 2 [Figs. 14(e) and 14(f)] and 4 [Figs. 14(g) and 14(h)]. The void at location 3 does not lead to the formation of a high-strength hot spot and no reaction initiation is observed at that location [Figs. 14(e) and 14(f)]. The behavior of all four voids in this real mesostructure is consistent with the predictions from the numerical experiments of idealized single elongated voids.

V. CONCLUSION

Using reactive mesoscale simulations, this work analyzed the sensitivity behavior of elongated voids that are prevalent in real mesostructures of pressed explosives. The effects of void orientations and aspect ratios on reaction initiation were studied. The understanding developed from the numerical simulations was shown to be useful in the prediction of reaction initiation and ignition locations in real mesostructures of pressed explosives. This was demonstrated by performing mesoscale analysis of a given sample of coarse-grained pressed explosives categorized as class III explosives. The key observations and insights obtained from the current work are itemized as follows.

(1) It was shown that coarse grids underpredict the hot spot temperatures and can lead to incorrect ignition threshold predictions. In general, 40 grid points across the elongated void thickness were found to be adequate to obtain a converged solution for an accurate reactive mesoscale simulation.

(2) It was shown that elongated voids are more sensitive and generate higher-strength hot spots when compared to cylindrical voids. This difference in the behavior of cylindrical and elongated void is connected to the physical mechanisms governing the collapse of voids of different shapes. Cylindrical voids collapse under the application of shock load, leading to the formation of material jets. Elongated voids collapse by a pinching mechanism, leading to the subsequent collapse of one surface of the void on the opposing surface. Each pinching instance generates blast waves. As the collapse progresses along the length of the void, the blast waves intensify and cause the formation of high-strength hot spots. This self-strengthening mechanism is not present in the situation involving a cylindrical void, which makes it less sensitive when compared to elongated voids.

(3) Elongated voids of various orientations and aspect ratios are present in the real mesostructure of the pressed explosives. It was shown that voids oriented at an angle less than 45° with respect to the incident shock wave are more sensitive. There are two competing mechanisms that operate during the collapse of arbitrarily oriented elongated voids: pinching mechanisms causing the collapse of the voids and rarefaction effects because of the shock reflection from the free surface of the voids when the incident shock impacts it. For orientations less than 45° the pinching mechanism dominates over the rarefaction effects and causes the voids to be sensitive.

(4) Elongated voids of aspect ratio greater than or equal to 5 were found to be more sensitive when compared to the low-aspect-ratio voids. Material jetting is the primary collapse mechanism that causes the collapse of the low aspect ratio, i.e., thicker voids. The self-strengthening pinching mechanism is the governing mechanism for the collapse of high-aspect-ratio voids, i.e., thinner voids, which makes the high-aspect-ratio void more sensitive.

The understanding of the sensitivity behavior of elongated voids was applied to predict critical void locations in the real mesostructure of a class III pressed explosive samples. The prediction of which voids are most sensitive can be made fairly robustly on the basis on their orientation and aspect ratio. This work therefore enables insights and physical mechanisms derived from mesoscale simulations to be used to predict the behavior of real mesoscale geometries.

The current work enhances the understanding of the behavior of pressed explosives under certain assumptions and limitations. The voids are modeled in two dimensions, whereas it is important to understand three-dimensional (3D) effects on the sensitivity behavior of elongated voids.

A preliminary attempt to distinguish 2D versus 3D physics of void collapse was presented in previous work [9]. Further consideration of three-dimensional effects is left for future work. Also, the current work demonstrates that the numerical experiments on elongated voids can predict critical locations for initiation in a real mesostructure. Mesoscale computations of real mesostructures are expensive. Therefore, it may be advantageous to develop an approach that can quantify the sensitivity of a given mesoscale sample by correlating sensitivity with mesoscale morphology. This requires a framework to quantify the local mesostructural morphological features in a given sample. To this end, ongoing work is aimed at developing an image analysis tool that can quantify global morphological metrics (particle size, shape, and proximity distributions) and local metrics (void orientations, aspect ratios, and correlation functions) and to relate the morphological metrics to sample sensitivity.

ACKNOWLEDGMENTS

This work was performed under grants from the AFOSR Computational Mathematics program, AFOSR Energetics Materials Program, and the AFRL-RWPC (Computational Mechanics Branch, Eglin AFB).

---

[1] E. J. Welle, C. D. Molek, R. R. Wixom, and P. Samuels, Microstructural effects on the ignition behavior of HMX, J. Phys.: Conf. Ser. **500**, 052049 (2014).

[2] B. A. Khasainov, A. A. Borisov, B. S. Ermolaev, and A. I. Korotkov, in *Proceedings of the 7th International Symposium on Detonation, Annapolis, MD* (Office of Naval Research, Annapolis, 1981), pp. 435–447.

[3] J. E. Field, Hot spot ignition mechanisms for explosives, Acc. Chem. Res. **25**, 489 (1992).

[4] R. Menikoff, in *Proceedings of the Conference of the American Physical Society Topical Group on Shock Compression of Condensed Matter*, AIP Conf. Proc. No. 706 (AIP, New York, 2004), p. 393.

[5] L. Tran and H. S. Udaykumar, Simulation of void collapse in an energetic material, Part I: Inert case, J. Propuls. Power **22**, 947 (2006).

[6] L. Tran and H. S. Udaykumar, Simulation of void collapse in an energetic material, Part 2: Reactive case, J. Propuls. Power **22**, 959 (2006).

[7] A. Kapahi and H. S. Udaykumar, Dynamics of void collapse in shocked energetic materials: Physics of void-void interactions, Shock Waves **23**, 537 (2013).

[8] G. A. Levesque and P. Vitello, The effect of pore morphology on hot spot temperature, Propellants Explos. Pyrotech. **40**, 303 (2015).

[9] A. Kapahi and H. S. Udaykumar, Three-dimensional simulations of dynamics of void collapse in energetic materials, Shock Waves **25**, 177 (2015).

[10] N. K. Rai and H. S. Udaykumar, Mesoscale simulation of reactive pressed energetic materials under shock loading, J. Appl. Phys. **118**, 245905 (2015).

[11] A. K. Kapila, D. W. Schwendeman, J. R. Gambino, and W. D. Henshaw, A numerical study of the dynamics of detonation initiated by cavity collapse, Shock Waves **25**, 545 (2015).

[12] H. Springer, C. Tarver, and S. Bastea, in *Proceedings of the Conference of the American Physical Society Topical Group on Shock Compression of Condensed Matter*, AIP Conf. Proc. No. 1793 (AIP, New York, 2015).

[13] A. B. Swantek and J. M. Austin, Collapse of void arrays under stress wave loading, J. Fluid Mech. **649**, 399 (2010).

[14] N. K. Bourne and J. E. Field, Bubble collapse and the initiation of explosion, Proc. R. Soc. A **435**, 423 (1991).

[15] N. K. Bourne and A. M. Milne, The temperature of a shock-collapsed cavity, Proc. R. Soc. A **459**, 1851 (2003).

[16] S. Sambasivan, A. Kapahi, and H. S. Udaykumar, Simulation of high speed impact, penetration and fragmentation problems on locally refined Cartesian grids, J. Comput. Phys. **235**, 334 (2013).

[17] A. Kapahi, S. Sambasivan, and H. S. Udaykumar, A three-dimensional sharp interface Cartesian grid method for solving high speed multi-material impact, penetration and fragmentation problems, J. Comput. Phys. **241**, 308 (2013).

[18] A. G. Kulikovskii, N. V. Pogorelov, and A. Y. Semenov, *Mathematical Aspects of Numerical Solution of Hyperbolic Systems* (CRC, Boca Raton, 2000).

[19] N. K. Rai, M. Schmidt, and H. S. Udaykumar, High-resolution simulations of cylindrical void collapse in energetic materials: Effect of primary and secondary collapse on initiation thresholds, following paper, Phys. Rev. Fluids **2**, 043202 (2017).

[20] C.-W. Shu and S. Osher, Efficient implementation of essentially non-oscillatory shock-capturing schemes, II, J. Comput. Phys. **83**, 32 (1989).

[21] S. Osher, Fronts propagating with curvature dependent speed algorithms based on Hamilton-Jacobi formulations, J. Comput. Phys. **79**, 12 (1988).

[22] R. P. Fedkiw, T. Aslam, B. Merriman, and S. Osher, A non-oscillatory Eulerian approach to interfaces in multimaterial flows (the ghost fluid method), J. Comput. Phys. **152**, 457 (1999).

[23] S. I. Dillard, J. A. Mousel, L. Shrestha, M. L. Raghavan, and S. C. Vigmostad, From medical images to flow computations without user-generated meshes, Int. J. Numer. Methods Biomed. Eng. **30**, 1057 (2014).